PHILOSOPHICAL TRANSACTIONS OF THE ROYAL SOCIETY A

Phil. Trans. R. Soc. A (2012) **370**, 208–234
doi:10.1098/rsta.2011.0178

Hydrodynamic principles of wave power extraction

By Chiang C. Mei*

Department of Civil and Environmental Engineering, Massachusetts Institute of Technology, Cambridge, MA 02139, USA

The hydrodynamic principles common to many wave power converters are reviewed via two representative systems. The first involves one or more floating bodies, and the second water oscillating in a fixed enclosure. It is shown that the prevailing basis is impedance matching and resonance, for which the typical analysis can be illustrated for a single buoy and for an oscillating water column. We then examine the mechanics of a more recent design involving a compact array of small buoys that are not resonated. Its theoretical potential is compared with that of a large buoy of equal volume. A simple theory is also given for a two-dimensional array of small buoys in well-separated rows parallel to a coast. The effects of coastline on a land-based oscillating water column are examined analytically. Possible benefits of moderate to large column sizes are explored. Strategies for broadening the frequency bandwidth of high efficiency by controlling the power-takeoff system are discussed.

Keywords: wave power; energy from ocean waves; water-wave scattering and radiation; wave–body interaction

1. Introduction

Despite the abundance of wave power in the sea, technologies for its extraction share with offshore wind power at least two similar challenges, i.e. unsteadiness in the supply and survivability of installations in stormy weather. To varying degrees of success, mastering these two challenges has been among the major objectives of research and development. There are now many different designs of wave energy converters (WECs). One type is to use waves to send water to an elevated reservoir. The stored water is then released through a turbine at a lower elevation. Tapchan, Oyster and Wave Dragon belong to this category. Others convert wave energy directly to the oscillatory motion of a rigid body, which then drives a linear generator. The body can be a cam [1], a buoy [2], an Archimedes wave swing or a series of rafts hinged together at the ends (Hagen–Cockerell raft and Pelamis). Alternatively, waves can also excite oscillations of the water surface inside a fixed chamber and force the air above through a turbine. Limpet, Pico

*ccmei@mit.edu

One contribution of 18 to a Theo Murphy Meeting Issue ‘The peaks and troughs of wave energy: the dreams and the reality’.

Table 1. Order estimate of power flux per unit length of wavefront.

amplitude (m)	power flux ($\mathrm{kW\,m^{-1}}$)
0.5	10
1	40
2	160

Plant and Mighty Whale have demonstrated the versatility of the oscillating water column (OWC) in various configurations. Devices involving flexible structures such as airbags [3] and bulging pipes [4] have also been proposed.

The ingenuity of many inventors has stimulated a large body of theoretical research to provide a sound and quantitative basis for these designs. Extensive surveys of the underlying theories as well as the history and progresses can be found in monographs [5–9], and in survey articles [10,11]. In this article, we only review some hydrodynamic principles and describe a few recent efforts, based exclusively on linearized theory. Computational methods and the mooring systems are left out. Nonlinear theories that are crucial to the survivability of WECs in stormy seas are still in progress, and are not discussed.

2. Power in ocean waves

Although much wave energy exists in deep seas far away from the coast, the high cost of construction, maintenance, transmission and storage makes it preferable to install WECs near the shore. By the physics of refraction, the propagation speed of a long-crested progressive wave decreases with decreasing water depth. Hence, incident waves from different directions in deep sea tend to approach a shallow coast normally. For a crude estimate, let us consider a plane wave of amplitude A and frequency ω. The rate of power flux across one unit length of the wavefront is

$$P = \tfrac{1}{2}\rho g|A|^2 C_{\mathrm{g}}, \tag{2.1}$$

where C_{g} is the group velocity,

$$C_{\mathrm{g}} = \frac{\omega}{2k}\left(1 + \frac{2kh}{\sinh 2kh}\right), \tag{2.2}$$

related to the wavenumber k and the local sea depth h by the dispersion relation

$$\omega^2 = gk \tanh kh. \tag{2.3}$$

For a typical period of $T = 10\,\mathrm{s}$, the power available is estimated for several amplitudes based on (2.1), as shown in table 1. In real seas, waves are irregular and broad-banded. We may regard A as the significant wave amplitude and ω the spectral peak frequency. The above estimate is of course highly simplistic, without due account of weather-related variabilities. Based on statistical data, Thorpe [12] has estimated the wave power potential along various coasts in the world ocean, as cited in figure 1. Based on the medium potential of $40\,\mathrm{kW\,m^{-1}}$, all the wave energy along 25 km of a coastline must be captured to match the capacity of a conventional power plant ($\mathcal{O}(1\,\mathrm{GW})$).

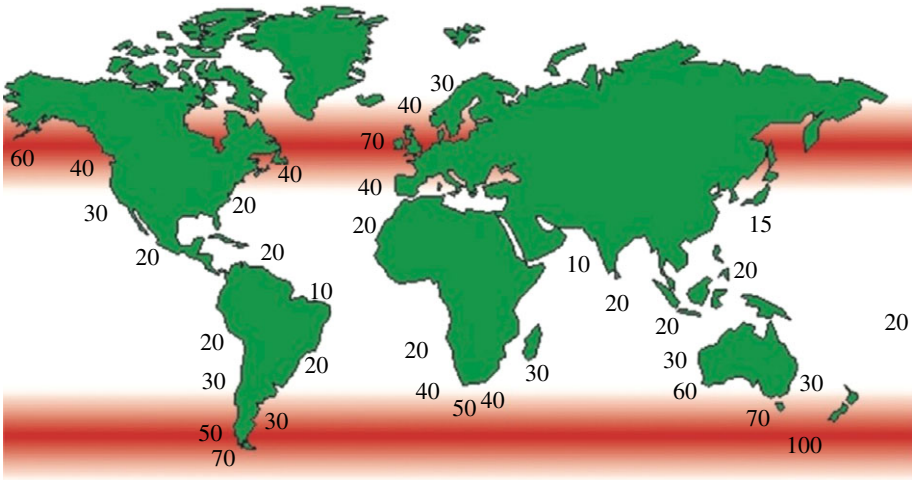

Figure 1. World's wave power potential in kW m^{-1}. Adapted from Thorpe [12]. (Online version in colour.)

3. Heuristic estimate of maximum efficiency

In a train of incoming waves, a converter scatters energy outwards simply by its presence, and also radiates energy by its motion. If by proper design of the system, the radiated waves are made to cancel most of the scattered waves, absorption efficiency can be high. The ground-breaking invention by Salter [1] illustrates this point clearly. Energy is transferred from waves to the power-takeoff device by the rolling motion of a long cam about a horizontal axis. With a circular stern of large enough radius and a pointed bow, the cam reflects almost all the incident waves and allows little transmission. By synchronizing its rolling motion, waves radiated against the incident waves can cancel the reflected waves to achieve complete absorption.

For a horizontal cylinder with a symmetrical cross section, cancellation of incident waves can be achieved by allowing two modes of oscillatory motion, e.g. heave and surge. Let the reflected and transmitted wave amplitudes be RA on the incidence side $x \sim -\infty$ and TA on the transmission side $x \sim \infty$. The amplitudes of radiated waves owing to heave are symmetric (Aa_{H}) on both sides, while those owing to surge are antisymmetric ($\pm Aa_{\mathrm{R}}$ as $x \to \pm\infty$). Cancellation of all outgoing waves on both sides $x \to \pm\infty$ is possible if $R + a_{\mathrm{H}} - a_{\mathrm{R}} = 0$ and $T + a_{\mathrm{H}} + a_{\mathrm{R}} = 0$, from which the factors a_{H} and a_{R} can be uniquely solved. Hence, total absorption is also possible in principle.

The simplest three-dimensional absorber is a circular buoy, as shown in figure 2. With the time factor $\mathrm{e}^{-\mathrm{i}\omega t}$ omitted, the free-surface displacement of the plane incident wave η_{I} can be decomposed as a sum of various angular modes,

$$\eta_{\mathrm{I}} = A\mathrm{e}^{\mathrm{i}kx} = A\sum_{n=0}^{\infty} \epsilon_n \mathrm{i}^n J_n(kr)\cos n\theta, \tag{3.1}$$

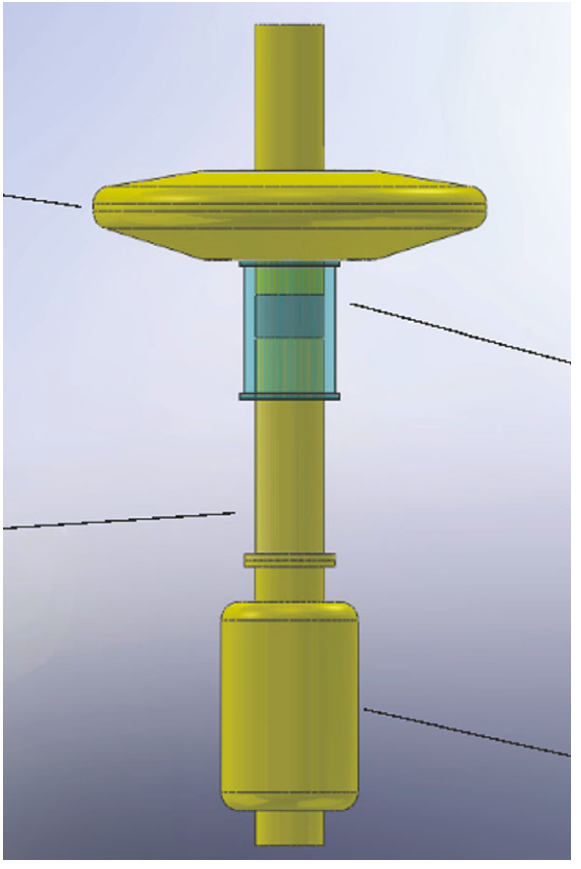

Figure 2. A typical buoy for wave power extraction. The tall spar-buoy serves as the shaft and provides stability. In waves, the disc-like buoy on the sea surface slides up and down the vertical shaft, and produces electricity through a linear generator. From http://www.ece.oregonstate.edu/wesrf, Prof. Annette von Jouanne, Oregon State University. (Online version in colour.)

where $\epsilon_0 = 1, \epsilon_n = 2, n = 1, 2, 3, \ldots$. For large kr, the nth angular mode in the sum above consists of a pair of radially incoming and outgoing waves,

$$\epsilon_n \frac{A}{2}\sqrt{\frac{2}{\pi kr}}\left[\mathrm{e}^{\mathrm{i}(kr-\pi/4-n\pi/2)} + \mathrm{e}^{-\mathrm{i}(kr-\pi/4-n\pi/2)}\right]\cos n\theta, \quad kr \gg 1. \tag{3.2}$$

Across a large circular cylindrical surface encircling the buoy, the total energy outflux (or influx) from each outgoing (or incoming) mode is

$$\frac{\epsilon_n}{2k}\rho g|A|^2 C_{\mathrm{g}}. \tag{3.3}$$

Since the rate of energy influx per unit length of the incident wavefront is given by (2.1), the capture width L is ϵ_n/k for mode n. For a circular buoy with a vertical axis, total cancellation of the isotropic outgoing mode ($n = 0$) can be achieved by the heave motion alone. On the other hand, the outgoing mode with $n = 1$ can be cancelled by the surge motion. Thus, the maximum possible capture width L is $1/k$ with optimal heave and $2/k$ with optimal surge, and $3/k$ with both [6,13].

4. Typical analysis for energy conversion by oscillating bodies

As will be reviewed later, to achieve the maximum efficiency by judicious cancellations, the basic strategy is to adjust the impedance of the device. Specifically, the WEC must first be resonated at the design frequency (e.g. the frequency at the peak of the incident wave spectrum). Second, the extraction rate of the power-takeoff system must be neither too small nor too large. Within the framework of the linearized potential theory, the analysis involves two parts: the wave hydrodynamics around the converter and the dynamics of the converter including the power-takeoff system. Taking a single floating body for illustration, the hydrodynamics consists of wave diffraction by the stationary body, and wave radiation owing to the forced motion of the body. Using linearity, the radiation problem for each forced mode is first solved for unit velocity (or displacement) amplitude. The amplitudes of all modes are then found from the dynamic equations of the body, after accounting for forces from diffraction and radiation of waves, and for coupling with power-takeoff and mooring systems.

The boundary-value problems involved can be stated for simple harmonic motion as follows. The amplitude of the velocity potential, defined by

$$\boldsymbol{u}(x,y,z,t)=\nabla\Psi(x,y,z,t)=\mathrm{Re}(\nabla\Phi(\boldsymbol{x})\,\mathrm{e}^{-\mathrm{i}\omega t}), \tag{4.1}$$

satisfies Laplace's equation in water,

$$\nabla^2\Phi=0,\quad \boldsymbol{x}\in\text{water}, \tag{4.2}$$

and the boundary condition on the free surface S_f,

$$\frac{\partial\Phi}{\partial z}-\frac{\omega^2}{g}\Phi=0,\quad (x,y)\in S_\mathrm{f}\ (z=0). \tag{4.3}$$

On the surface of the rigid structure S_B, the normal velocity must be continuous,

$$\frac{\partial\Phi}{\partial n}=\sum_\alpha n_\alpha V_\alpha,\quad \boldsymbol{x}\in S_\mathrm{B}, \tag{4.4}$$

where V_α is the amplitude of the body velocity in the generalized mode α (heave, sway, surge, etc.), and n_i is the generalized unit normal pointing into the body. In the far field, the incident wave

$$\varphi_\mathrm{I}=-\frac{\mathrm{i}gA}{\omega}\,\mathrm{e}^{\mathrm{i}kx}\frac{\cosh k(z+h)}{\cosh kh} \tag{4.5}$$

induces scattered waves by the presence, and radiated waves by the body motion. Both waves must be outgoing in the far field. These potentials can be solved separately from the body velocities.

To find V_α, one must consider the dynamics of the body, with additional account of the reaction forces from the power-takeoff and the mooring systems.

5. An isolated buoy converter

As an example, let us consider an axially symmetric buoy attached to a stationary electric generator. Making use of linearity, we decompose the total potential into

two parts, representing diffraction (φ) and radiation (ϕ),

$$\Phi = \varphi + \phi. \tag{5.1}$$

Each potential satisfies (4.2) throughout the sea water. On the wetted body surface, the diffracted wave must satisfy the no-flux condition

$$\frac{\partial \varphi}{\partial n} = 0, \quad \boldsymbol{x} \in S_{\mathrm{B}}, \tag{5.2}$$

since the body is stationary. Let the radiation potential be decomposed into three generalized modes (heave, sway and surge),

$$\phi = \sum_{\alpha=1}^{3} V_\alpha \phi_\alpha. \tag{5.3}$$

For each radiation mode, the body oscillates at unit normal velocity

$$\frac{\partial \phi_\alpha}{\partial n} = n_\alpha, \tag{5.4}$$

where n_α is the generalized unit normal. In the far field, $kr \gg 1$, the scattered $\varphi_{\mathrm{S}} = \varphi - \varphi_{\mathrm{I}}$ and the radiated wave ϕ_α must behave as outgoing waves

$$\sqrt{kr}\left(\frac{\partial}{\partial r} - \mathrm{i}k\right)[(\varphi - \varphi_{\mathrm{I}}), \phi_\alpha] \to 0, \quad kr \gg 1. \tag{5.5}$$

For any general geometry, there are now several effective numerical schemes to solve the boundary-value problems for these potentials (WAMIT, hybrid elements, etc.). Afterwards, the diffraction (exciting) force can be computed by integrating the dynamic pressure over the wetted body surface,

$$F_\alpha^{\mathrm{D}} = \mathrm{i}\rho\omega \iint_{S_{\mathrm{B}}} \varphi \, n_\alpha \, \mathrm{d}S. \tag{5.6}$$

From the radiation potential due to unit motion of mode β, i.e. ϕ_β, the αth component of the hydrodynamic reaction on the body can also be computed,

$$f_{\beta\alpha} = \mathrm{i}\rho\omega \iint_{S_{\mathrm{B}}} \phi_\beta n_\alpha \, \mathrm{d}S, \tag{5.7}$$

which is complex. The imaginary part of this complex reaction defines the matrix of apparent inertia

$$\mu_{\beta\alpha} = \frac{1}{\omega}\mathrm{Im} f_{\beta\alpha}, \tag{5.8}$$

while the real part defines the radiation damping matrix

$$\lambda_{\beta\alpha} = -\mathrm{Re} f_{\beta\alpha}. \tag{5.9}$$

Let us define the displacement component X_β by including the time factor,

$$\frac{\mathrm{d}X_\beta}{\mathrm{d}t} = \mathrm{Re}(V_\beta \, \mathrm{e}^{-\mathrm{i}\omega t}), \quad X_\beta = \mathrm{Re}(\xi_\beta \, \mathrm{e}^{-\mathrm{i}\omega t}), \tag{5.10}$$

then the total hydrodynamic reaction is

$$F_\alpha^{\mathrm{R}} = \sum_\beta [\omega^2 \mu_{\beta\alpha} + \mathrm{i}\omega\lambda_{\beta\alpha}]\xi_\beta. \tag{5.11}$$

The power-takeoff device exerts a reaction force on the body in the direction α. In general, it can contain inertial, elastic and damping forces. For simplicity, all these forces are modelled by terms linear in body displacement or velocity. For sinusoidal motion, the total reaction can be expressed as

$$(\omega^2 \mu'_{\alpha\beta} - C'_{\alpha\beta} + \mathrm{i}\omega\lambda'_{\alpha\beta})\xi_\beta, \tag{5.12}$$

where $\mu'_{\alpha\beta}$ is the inertia, $C'_{\alpha\beta}$ the elasticity and $\lambda'_{\alpha\beta}$ the extraction rate. One must then solve for the body displacements ξ_β of the floating buoy from Newton's law,

$$[-\omega^2(M + \mu_{\alpha\beta} + \mu'_{\alpha\beta}) + (C_{\alpha\beta} + C'_{\alpha\beta}) - \mathrm{i}\omega(\lambda_{\alpha\beta} + \lambda'_{\alpha\beta})]\xi_\beta = F_\alpha^{\mathrm{D}} + \mathscr{F}_\alpha, \tag{5.13}$$

where M is the static buoyant mass, $C_{\alpha\beta}$ is the restoring force matrix owing to buoyancy and $\mathscr{F}_\alpha$ denotes the mooring force.

Once ξ_β is solved, the total rate of power extraction can be obtained.

For the same frequency, the boundary-value problems for diffraction and radiation are similar, and can be solved by the same numerical scheme. To check the correctness and accuracy of computations, use can be made of a number of integral identities that can be deduced by applying Green's formula to a pair of wave potentials over a large fluid domain surrounding the body [13,14]. For example, by choosing a pair of two radiation potentials, $(\phi_\alpha, \phi_\beta)$, one can prove the symmetry of apparent inertia and damping matrices. From a diffraction potential and a radiation potential, one gets Haskind's relation, which can be used to derive the following identity between the exciting force and the radiation damping coefficient,

$$\lambda_{\alpha\alpha} = \frac{k/8\pi}{\rho g C_{\mathrm{g}} |A|^2} \int_0^{2\pi} |F_\alpha^{\mathrm{D}}(\theta)|^2 \, \mathrm{d}\theta. \tag{5.14}$$

By choosing the diffraction potential $\varphi = \varphi_{\mathrm{I}} + \varphi_{\mathrm{S}}$ and its own complex conjugate, φ, φ^*, one gets the law of conservation of mechanical energy, etc. These identities are also useful for physical insight and for theoretical analysis [6,7].

For quantitative insight, we now consider an idealized circular buoy heaving in a sea of constant depth h as sketched in figure 3 [2]. For this simple geometry, the scattered and heave-induced radiated waves can be found by eigenfunction expansions. In particular, the radiated wave is isotropic in all horizontal directions. Let the heave displacement be $Z = \mathrm{Re}(\zeta \, \mathrm{e}^{-\mathrm{i}\omega t})$. Assuming for simplicity that the power-takeoff system exerts only a damping force on the buoy, the buoy displacement ζ is governed by

$$-M\omega^2\zeta = F_z^{\mathrm{D}} + \omega^2 \mu_{zz}\zeta - \mathrm{i}\omega\zeta(\lambda_{zz} + \lambda_{\mathrm{g}}) + \rho g \pi a^2 \zeta, \tag{5.15}$$

where $\lambda_{\mathrm{g}} \equiv \lambda'_{zz}$. Hence, the buoy displacement is

$$\zeta = \frac{F_z^{\mathrm{D}}}{\rho g \pi a^2 - \omega^2(M + \mu_{zz}) - \mathrm{i}\omega(\lambda_{\mathrm{g}} + \lambda_{zz})}. \tag{5.16}$$

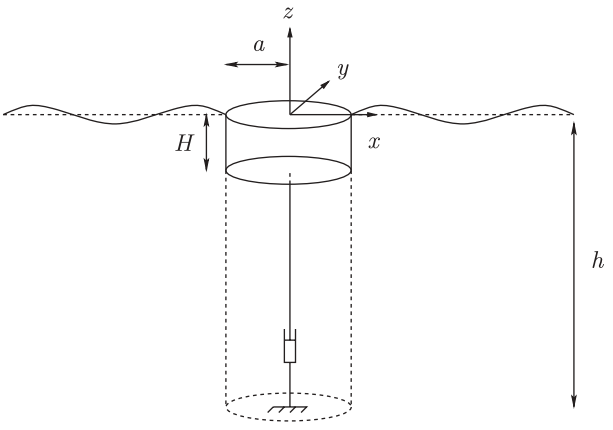

Figure 3. Sketch of the system. Energy extractor is symbolized by the dashpot.

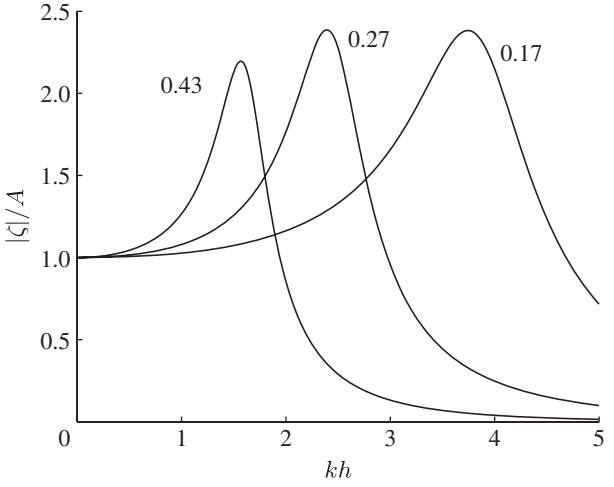

Figure 4. Normalized amplitude of the buoy displacement for three buoys with $a/h = 0.17, 0.27, 0.43$. The draft H of each buoy is equal to the radius a. The coefficient λ_g is chosen such that energy extraction is the greatest at resonance. Adapted from Garnaud & Mei [19].

From the numerical solution of the scattering and radiation problems for a buoy with equal radius and draft, the dimensionless amplitude of the buoy displacement on the depth-to-wavelength ratio kh is plotted in figure 4. Note that for a larger buoy, the peak of resonance occurs at a lower $k = k_R$, or longer waves. In a sea of depth $h = 15\,\mathrm{m}$, the resonance wave periods for $a/h = 0.43, 0.27, 0.17$ are $8, 5, 4\,\mathrm{s}$, respectively (figures 4 and 5). The bandwidth of resonance is also narrower. It can be estimated that the peak frequency is roughly inversely proportional to the buoy radius, i.e. $k_R a = \mathcal{O}(1)$.

The rate of power extracted is

$$P = \frac{1}{2}\lambda_g \omega^2 |\zeta|^2 = \frac{1}{2}\frac{\lambda_g \omega^2 |F_z^D|^2}{(\rho g \pi a^2 - \omega^2(M + \mu_{zz}))^2 + \omega^2(\lambda_g + \lambda_{zz})^2}. \tag{5.17}$$

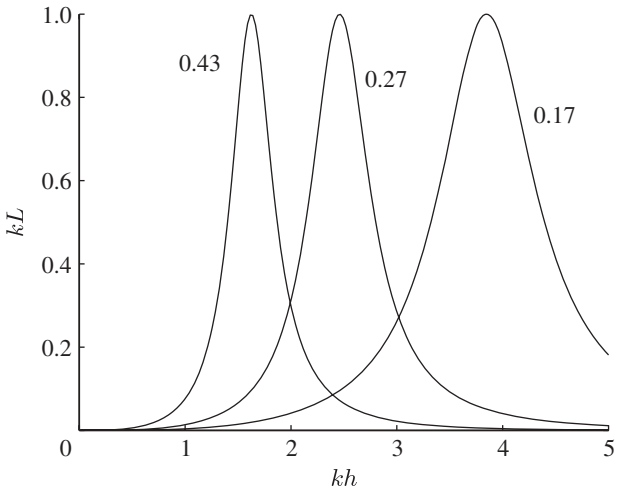

Figure 5. Energy extraction and buoy movement for three different sizes of buoys with $a = H$. The dimensionless energy extraction rate λ_g is constant and chosen such that the energy extraction is maximum at resonance, and the ratio a/h is shown next to the curves. Adapted from Garnaud & Mei [19].

Dividing P by the power influx across a unit width of the incident wavefront leads to the capture width L

$$kL = \frac{k}{C_g} \frac{\lambda_g \omega^2 |F_z^D|^2/(\rho g A^2/2)}{\omega^2(\lambda_{zz} + \lambda_g)^2 + (\rho g \pi a^2 - \omega^2(M + \mu_{zz}))^2}. \tag{5.18}$$

Conditions for maximum energy extraction are

$$\rho g \pi a^2 - \omega^2(M + \mu_{zz}) = 0, \tag{5.19}$$

i.e. resonance, and that the extraction rate equals the radiation damping rate

$$\lambda_g = \lambda_{zz}. \tag{5.20}$$

Making use of (5.14), equation (5.17) reduces to

$$P_{max} = \frac{1}{2k} \rho g |A|^2 C_g, \tag{5.21}$$

so that $kL_{max} = 1$.

It can be shown that this maximum occurs when $k_R a = \mathcal{O}(1)$. If resonance is desired at a low frequency, the buoy must be sufficiently large, but then the bandwidth is small. It is difficult for a small buoy of a few metres radius to resonate at a wave period around 10 s and to have a wide bandwidth of high efficiency, without adding extra controls of the power-takeoff system.

At present, the estimated power-generating capacity of a single buoy is about 50–100 kW. Therefore, it would take 20–40 buoys to match a wind turbine of 2 MW capacity. How to arrange an array of many buoys must take account of the absorption efficiency, economy of materials, ease of maintenance and the acceptable size of the footprint. For 100 per cent efficiency or complete absorption of the incoming wave energy, one can in principle construct a linear array parallel to the wavefront if the buoys are separated at a distance of $\mathcal{O}(1/k)$. Budal [15] has

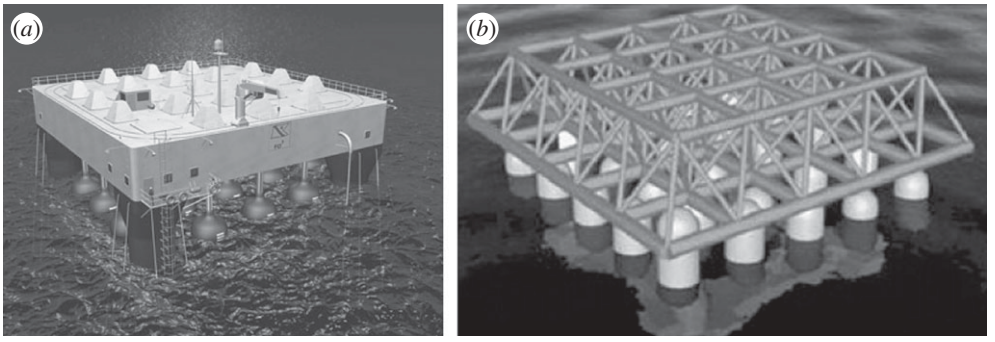

Figure 6. Compact arrays of buoys. (*a*) FO3 of Norway (from http://www.abb.com). (*b*) Manchester Bobber of UK (from http://www.manchesterbobber.com).

shown that for two parallel rows of linear arrays in normally incident waves, the spacing can be as large as $2\pi/k$ for perfect absorption, owing to interference of adjacent buoys. For four parallel lines of buoys, the spacing can be doubled [16]. Thus, for the same number of buoys, different array geometry can be considered to satisfy navigational and environmental constraints.

6. A compact array of small buoys

As mentioned in the previous section, a single buoy has a limited frequency band of high efficiency, and needs to be reasonably large to achieve resonance at a frequency typical of the spectral peak in coastal seas. To broaden the bandwidth, K. Budal & S. Salter have proposed phase control (see [17,18] for more recent accounts). An alternative answer seems to be provided by several recent designs based on the idea of a compact array of small buoys (figure 6). Fred Olsen of Norway (http://www.abb.com/) and Peter Stansby of UK (http://www.manchesterbobber.com/) have separately proposed similar designs by installing dozens of small buoys on a square rig (figure 6). The horizontal dimension of the rig is a sizeable fraction of a design wavelength, while the buoy diameter and spacing are much smaller. The projected capacity of one rig is about 2.5 MW, comparable with a wind turbine. WaveStar of Denmark (http://www.WaveStarEnergy.com/) is based on similar ideas and has the small buoys forming two linear arrays instead.

The main objective of a compact array of small buoys is to broaden the efficiency bandwidth. Optimum efficiency at any frequency is sacrificed by not attempting impedance matching. To examine the potential performance of such a design, a theory has been given by Garnaud & Mei [19,20]. Heuristically, a compact array of small buoys acts like a mat of dampers distributed over an area of the sea surface. The mathematical consequence is to change the free-surface boundary condition (4.3) to a different form. Referring to figure 7, let us consider one small buoy with $ka = \mathcal{O}(kH) \ll 1$. The linearized kinematic condition for the buoy displacement Z is

$$\frac{\partial Z}{\partial t} = \frac{\partial \Psi}{\partial z}, \quad z = 0, \tag{6.1}$$

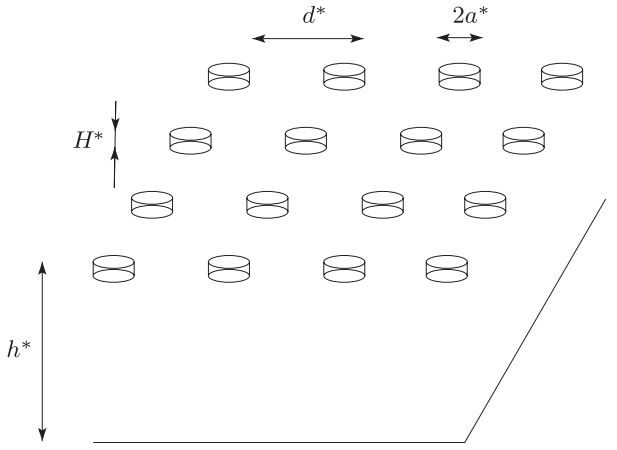

Figure 7. A compact array of small buoys. Adapted from Garnaud & Mei [19].

applied on the mean free surface because of the small draft. Assuming that all the small buoys have the same extraction rate λ_g, the dynamic condition on each buoy can be obtained by approximating (5.15) for small ka. First, radiation damping λ_{zz} is at most of the order $\mathcal{O}(k^2a^2)$ and negligible. The exciting force can be approximated by using the local pressure averaged over the buoy bottom $-\rho g\pi a^2(\partial\Psi/\partial t)$. Furthermore, by the Archimedes principle, $M=\rho\pi a^2H$, hence the ratio of inertia to buoyancy is small, $M\omega^2/\rho g\pi a^2=\omega^2H/g=\mathcal{O}(kH)\ll 1$. The apparent mass is at best of the same order as the actual mass, hence is likewise small. Assuming that the extraction rate λ_g is not small, i.e. much greater than the radiation damping rate, the dynamic condition is simply

$$0=-\rho g\pi a^2 Z-\lambda_g\frac{\partial Z}{\partial t}-\rho\pi a^2\frac{\partial\Psi}{\partial t},\quad z=0, \tag{6.2}$$

to the leading order. Furthermore, as the wavelength is much larger than the size of the buoy, the averaged potential (Ψ) differs little from the local potential Ψ. After eliminating Z, we get

$$\left(\frac{\lambda_g}{\rho g\pi a^2}\frac{\partial}{\partial t}+1\right)\frac{\partial\Psi}{\partial z}+\frac{1}{g}\frac{\partial^2\Psi}{\partial t^2}=0,\quad z=0. \tag{6.3}$$

It follows for simple harmonic motion that

$$\frac{\partial\Phi}{\partial z}-\frac{\omega^2/g}{1-(\mathrm{i}\lambda_g\omega/\rho g\pi a^2)}\Phi=0,\quad z=0, \tag{6.4}$$

which holds under each buoy.

Over the free surface in the open water surrounding the buoy, the boundary condition is obtained by taking $\lambda_g=0$. The corresponding body displacement is

$$Z=\mathrm{Re}(\zeta\,\mathrm{e}^{-\mathrm{i}\omega t}),\quad \zeta=\frac{\mathrm{i}\omega\Phi|_{z=0}}{1-(\mathrm{i}\lambda_g\omega/\rho g\pi a^2)}. \tag{6.5}$$

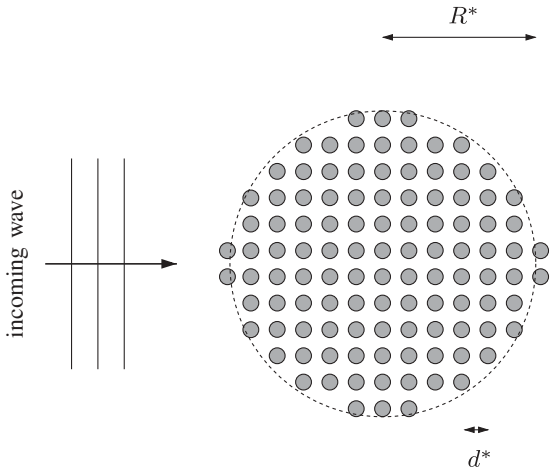

Figure 8. A circular array of energy-absorbing buoys.

Now consider the coarse scale comparable with a wavelength. Let $f \equiv \pi a^2/d^2$ be the area fraction covered by buoys, which is in the range of $0 < f < \pi/4$ for circular cylinders in a square array since $a \leq d/2$. The averaged free-surface condition[1] is

$$(1-f)\left(\frac{\partial \Phi}{\partial z} - \frac{\omega^2}{g}\Phi\right) + f\left(\frac{\partial \Phi}{\partial z} - \frac{\omega^2/g}{1-(\mathrm{i}\lambda_{\mathrm{g}}\omega/\rho g \pi a^2)}\Phi\right) = 0, \tag{6.6}$$

or

$$\frac{\partial \Phi}{\partial z} - \frac{\omega^2}{g}[1 + f(\mathcal{F}_0 - 1)]\Phi = 0, \tag{6.7}$$

where

$$\mathcal{F}_0(\omega) = \frac{1}{1-(\mathrm{i}\lambda_{\mathrm{g}}\omega/\rho g \pi a^2)} \tag{6.8}$$

expresses the effect of the energy absorber. Note that only the area fraction f matters and the small buoy draft is immaterial. Equation (6.7) can be derived by the more systematic asymptotic method of multiple scales [19].

With the familiar boundary condition over the sea surface uncovered by buoy rigs, we can now solve the coarse-scale boundary-value problem for the interaction between waves and the rig. Continuity of pressure and normal velocity must be required along the vertical cylindrical surface separating the buoys and the open water. For a circular rig of radius R, as shown in figure 8, the boundary-value problem can be solved by separation of variables involving vertical eigenfunctions corresponding to the eigenvalues that are the complex roots $k_n, n = 1, 2, 3, \ldots$ of the transcendental relation

$$\omega^2(f\mathcal{F}_0(\omega) + (1-f)) = gk\tanh(kh). \tag{6.9}$$

[1]It can be easily modified for the sea surface covered with small ice floes.

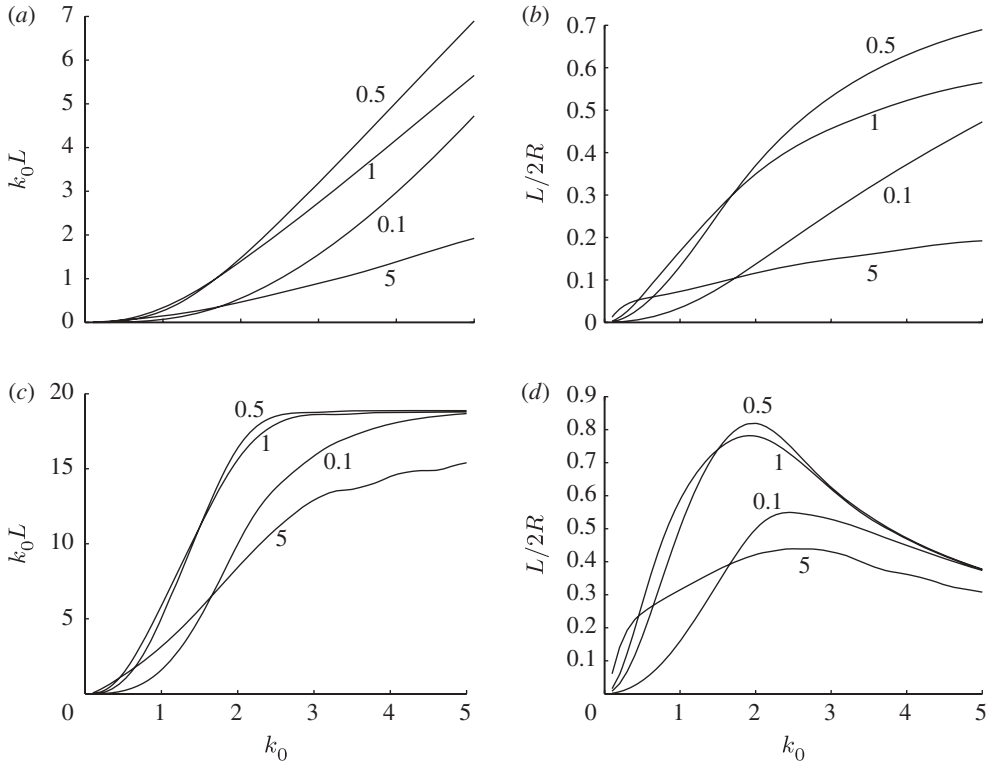

Figure 9. Dependence of effectiveness on the extraction rate λ whose values are indicated next to the curves. The packing ratio is $f = 0.2$. (*a*) $R = 1$, (*b*) $R = 1$, (*c*) $R = 5$, (*d*) $R = 5$. Adapted from Garnaud & Mei [19].

The effects of varying extraction rates on the capture width are shown for two arbitrarily chosen array sizes in figure 9. The dimensionless extraction rate is defined by

$$\bar{\lambda}_{\mathrm{g}} = \frac{\lambda_{\mathrm{g}}}{\rho\sqrt{gh}\pi a^2}. \tag{6.10}$$

Not relying on resonance, the array does not suffer the shortcoming of narrow-bandedness of an isolated large buoy. The ratio of capture length to the array radius R is less than 100 per cent, however, the bandwidth is not sharply peaked as that of a large single buoy. Note that the efficiency approaches a finite limit as kh increases, and the limit is reached at smaller kh for larger R/h. As expected, the larger array extracts more energy at low frequencies, similar to an isolated large buoy. Note also that the extraction rate has to be of certain intermediate value (here approx. 0.5) for the efficiency to be the best. We caution however that these computed results are within the assumed bounds of small kH or ka only for relatively long waves, say, $kh < 2$. For shorter waves, the buoy inertia and radiation damping may need to be taken into account for more accurate prediction.

How is a compact array of small buoys compared with a single large buoy of equal volume? Let us consider a circular array of overall radius R and area fraction of solid f. The total volume of all small buoys in the array is $f\pi R^2 H$,

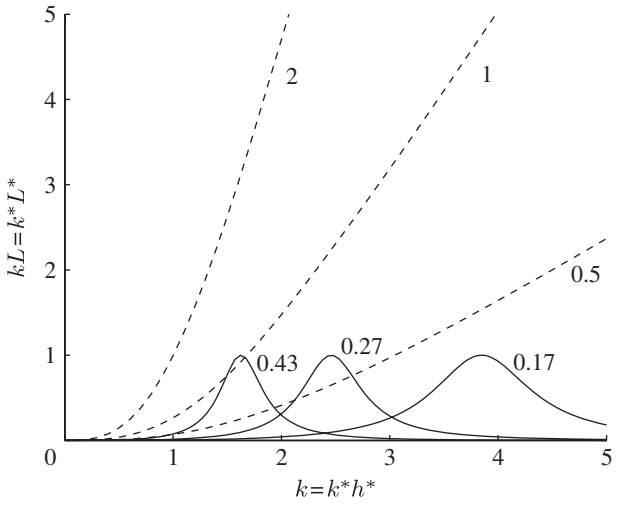

Figure 10. Comparison of capture widths of three circular arrays of small buoys with three large buoys of equal volume. Dashed curves represent the compact arrays with the same $f = 0.2$ and $\bar{\lambda}_g = 0.5$ and draft $H/h = 1/10$. The array radii are $R/h = 0.5, 1, 2$. Results for the corresponding large buoys (radius/draft: $a_b = (fR^2H/d)^{1/3} = 0.17, 0.27, 0.43$) are shown by solid curves. For each large buoy, the extraction rate is chosen to be the optimum at the peak. Adapted from Garnaud & Mei [19].

where H denotes the draft of each small buoy.[2] Let the radius and draft of the corresponding large buoy be a_b so that its volume is πa_b^3. Equating the two volumes, we get $a_b = (fR^2H)^{1/3}$. In figure 10, we fix $f = 0.2$ and $H = 0.1h$ and consider three arrays with $R = (0.5, 1.0, 2.0)h$. The corresponding large buoys have the radii and draft $a_b = (0.17, 0.27, 0.43)h$, respectively. Their capture widths are compared. It is clear that the compact array is hydrodynamically very promising as it can extract much more energy than a single buoy of equal volume, and with a much wider bandwidth. In reality, friction losses will likely be much greater for the compact array and reduce the efficiency predicted by the potential theory. Further experiments are needed.

Of course, additional technical challenges remain. For example, can the overall efficiency be improved by separately controlling the rate of energy extraction from each small buoy? To what extent does the rig movement influence energy extraction? What is the power potential of dozens or hundreds of these platforms in a large array? Aside from more accurate accounts of buoy inertia (real and added) and radiation damping by existing computational schemes, mooring systems, nonlinear effects of finite-amplitude waves and frictional loss owing to flow separation must all be considered for more comprehensive mathematical modelling of actual designs.These factors and the questions of cost and safety are worth further study.

[2]Recall that the performance of the compact buoy array does not depend on the buoy draft.

7. Many rows of small buoys

There have been many ideas of installing a large group of WECs either in clusters or in long rows parallel to the coastline. A long array of buoys has been studied theoretically by Budal [15] and Falnes & Budal [16]. Typically the units are separated by distances comparable with or greater than the incident wave length, i.e. $kb = \mathcal{O}(1)$. When the separation between buoys is comparable with a wavelength, resonance owing to their interaction may occur at some frequencies within the energetic part of the incident wave spectrum. Falcäo [21] found for a linear array of OWCs, that resonance occurs when $kb = 2n\pi(1 + \sin\alpha)$ and the efficiency vanishes, where α is the angle of incidence with $\alpha = 0$ corresponding to normal incidence.

As remarked at the end of §5, if a periodic array of buoys is lined in a row parallel to the coast, perfect extraction can be achieved if the spacing between adjacent buoys is properly chosen. The optimum spacing between two adjacent buoys in the same row can be increased by increasing the number of rows. To allow easy communications to and from the coast, one can in principle line up many parallel rows of buoys. Such a wave power farm can also be formed by many attenuators (lines of buoys perpendicular to the coast), such as Cockeral's rafts or Pelamis. The attenuators can be much farther apart than the spacing d between neighbouring buoys in the same attenuator, thereby facilitating navigation to and from the shore. This idea has been explored by Falnes [22] who considered the constructive interference between buoys and showed that for infinitely many lines of attenuators spaced at W apart, with N degrees of freedom per attenuator,[3] 100 per cent absorption of normally incident waves is possible if $N > 2 + 2kW/\pi$. In these theories, the buoy size is not small so that resonance can be induced for maximum extraction.

As an alternative to attenuators composed of several large buoys, Garnaud & Mei [23] considered an infinite number of parallel attenuators, each of which consisted of many small buoys. The attenuators were separated by the distance W, and the spacing d between neighbouring buoys in the same attenuator was assumed to be $d = \mathcal{O}(h) = \mathcal{O}(1/k)$. For normal incidence, the mathematical problem is equivalent to one attenuator along the centreline of a channel. They gave the following crude account of the physics by neglecting the influence of the neighbouring buoys. As the buoy size is much smaller than the incident wavelength, scattering is negligible and the diffraction pressure is dominated by $\rho g A$. Ignoring the small buoy mass, the vertical displacement of a single boy of small radius a and draft H is governed by (6.5), from which the period-averaged rate of energy extraction per buoy $\frac{1}{2}\omega^2\lambda_g|\zeta|^2$ is found. Dividing by the energy influx rate across the channel width W, the fraction of power extracted per unit time by one buoy is

$$\frac{(1/2)\omega^2\lambda_g|\zeta|^2}{(1/2)\rho g|A|^2 C_g W}. \tag{7.1}$$

Let us examine the macro-scale picture of many buoys. Since the density of buoys, i.e. the number of buoys per unit length, is $1/d$, the fractional rate of power

[3]For example, if all buoys can only heave, N is the total number of buoys in an attenuator.

extraction per unit macro-scale length is

$$\frac{1}{\mathcal{L}} = \frac{(1/2)\lambda_g \omega^2 |\zeta|^2}{(1/2)\rho g |A|^2 C_g W d} = \frac{\omega^2}{\rho g C_g W d} \frac{\lambda_g}{1 + (\omega \lambda_g / \pi a^2 \rho g)^2}. \tag{7.2}$$

The fraction of energy flux rate remaining at station dx is

$$F(x + dx) = F(x)\left(\frac{1 - dx}{\mathcal{L}}\right). \tag{7.3}$$

It follows after Taylor expansion that

$$\frac{\mathrm{d}F}{\mathrm{d}x} = -\frac{F}{\mathcal{L}}, \tag{7.4}$$

which has the solution

$$F = \mathrm{e}^{-x/\mathcal{L}}. \tag{7.5}$$

For a linear array of fixed total length X, the efficiency is

$$\mathcal{E}_0 = 1 - \mathrm{e}^{-X/\mathcal{L}}. \tag{7.6}$$

The total power extracted per attenuator is

$$P = \tfrac{1}{2}\rho g |A|^2 C_g W (1 - \mathrm{e}^{-X/\mathcal{L}}). \tag{7.7}$$

To save the cost of construction, $\mathcal{L}$ should be small. Clearly, when either $\lambda_g \to 0$ or $\lambda_g \to \infty$, $\mathcal{L} \to \infty$, both $\mathcal{E}_0$ and P vanish for a fixed X. For finite X, extremization with respect to λ_g gives the optimum rate

$$\lambda_g^{\mathrm{opt}} = \frac{\pi a^2 \rho g}{\omega}, \tag{7.8}$$

which must be larger for longer waves. For complete extraction of all wave power coming into the channel, the array length should be of the order of

$$\mathcal{L}_{\mathrm{opt}} = \frac{2W\, dC_g}{\pi a^2 \omega}, \tag{7.9}$$

which is large when compared with d or h, larger for longer waves, and of course must increase with W and d. The number of rows required is $\bar{N} = \mathcal{O}(\mathcal{L}_{\mathrm{opt}}/d)$, which increases with W. This result is similar to that in [22] for buoys of any size. Figure 11*a* shows the efficiency as a function of kh for one X and different extraction rates, while figure 11*b* shows the effects of array length X when the optimal extraction rate (7.8) is chosen for every ω, hence k. Again for short waves (e.g. $kh > 2$), the numerical results reported here may require improvement by accounting for buoy inertia and radiation damping.

Garnaud & Mei [23] also found that the preceding result holds only if the buoy spacing d is not close to the special value $kd = n\pi$, i.e. $d = n\pi/\lambda$, for an integer $n = 1, 2, 3, \ldots$. Otherwise, Bragg resonance happens so that even the weak effect of scattering by each buoy is accumulated to give rise to strong reflection. Buoys behind the front rows are shielded from the incident wave, leading to considerable drop of overall extraction efficiency. Fortunately, the loss occurs only in narrow bands around these discrete and relatively high frequencies. Details can be found in the study of Garnaud & Mei [23].

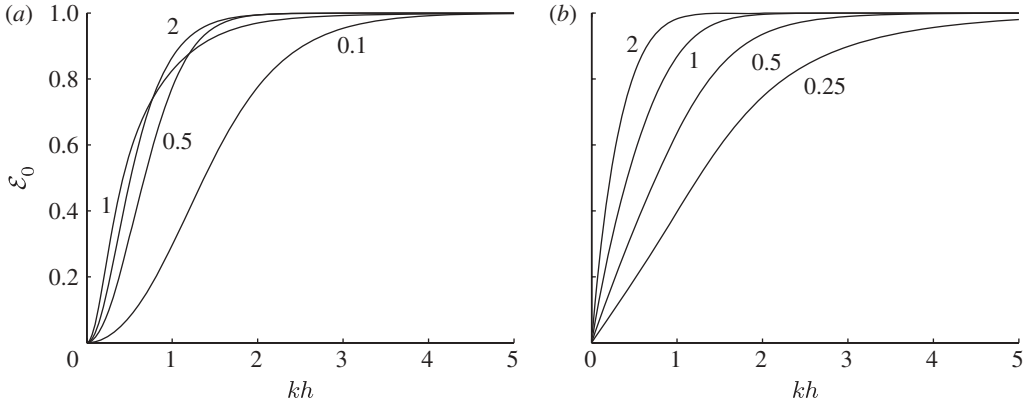

Figure 11. Energy extraction efficiency $\mathcal{E}_0$ versus kh for a square array with $d/h = 1$. (a) Effects of the dimensionless extraction rates $\bar{\lambda}_g = \lambda/(\rho g \pi a^2 \sqrt{gh}) = 0.1, 0.5, 1, 2$ for normalized array length $\bar{X} = (a^2/h)X = 1$. (b) Effects of complete optimization for every frequency, for $\bar{X} = 0.25, 0.5, 1, 2$. Adapted from Garnaud & Mei [23].

8. Oscillating water column on the coast

Savings in construction, maintenance, power transmission and storage are some of the reasons to build a wave energy system on land. A few years ago, there was a plan in Portugal for a full-scale OWC installed at the tip of a breakwater at the mouth of River Douro. While numerical modelling is needed to simulate the actual geometry, local bathymetry and the coastline, for physical insight, analytical studies have been made for the idealized geometries of an OWC at the tip of a very thin breakwater [24], or along the straight coast [25], or at a coastal corner [26]. The column is assumed to be a vertical cylinder of circular cross section, with an opening below the mean sea surface. One of the findings is that if the radius of a circular OWC is sufficiently large, the air chamber can serve the purpose of broadening the bandwidth of high efficiency. This result can be used to devise strategies for optimizing the power-takeoff characteristics.

Figure 12 depicts the idealized geometry where a circular column of radius a is centred at the tip of a wedge-like coast. In plane polar coordinates, the coastlines are defined by the rays $\theta = 0$ and $\nu\pi$ with $0 < \nu < 2$, so that the land mass is defined by $\nu\pi < \theta < 2\pi$, $r > a$. The column is open to the sea over the depth range $-h < z < -d$. Plane incident waves arrive from the angle α with respect to one coast ($\theta = 0$). Water inside the column rises and falls with the incoming waves and forces the air in the chamber above through one or several Wells turbines at the top. For simplicity, the cylinder wall has no thickness and the sea depth h is constant everywhere.

The dynamics of an OWC consists of wave diffraction by and radiation from the partially open column next to the coastline, and the compression and expansion of chamber air between the water surface and the Wells turbines. Leaving the mathematical details to earlier studies [24–26], we sketch the essential ideas below.

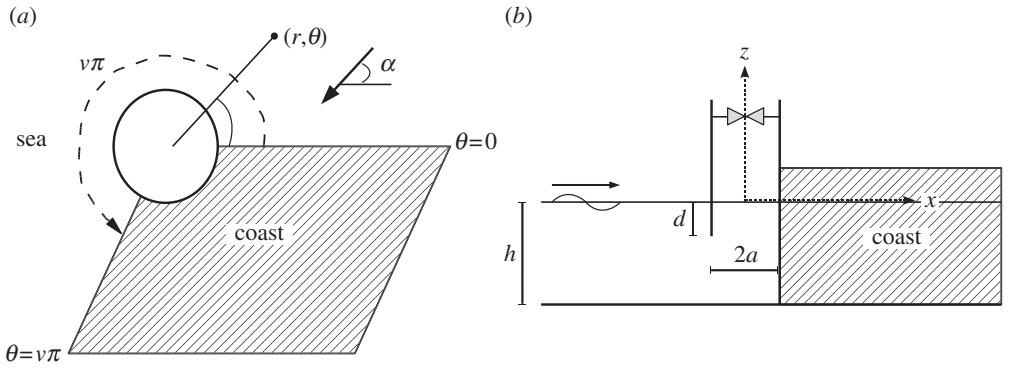

Figure 12. An OWC at the tip of a wedge-like coast. Incident plane waves arrive at angle α. (a) Top view. (b) Side view.

(a) *Power-takeoff*

Because of the relatively low frequency of water waves and the high speed of sound in air, the air pressure inside the chamber is virtually uniform. The mass flux rate of air through the turbines is proportional to the pressure difference across them. Assuming the chamber air to be compressible and its motion isentropic, then for simple harmonic motion of angular frequency ω, the complex amplitudes of the total volume flux rate $\hat{Q}$ and the air pressure $\hat{p}_{\rm a}$ are related by [27]

$$\hat{Q} = \left(\frac{KD}{N\rho_{\rm a}} - \frac{{\rm i}\omega V_0}{c_{\rm a}^2 \rho_{\rm a}} \right) \hat{p}_{\rm a}, \tag{8.1}$$

where $\hat{Q}$ and $\hat{p}_{\rm a}$ are the amplitudes of Q and $p_{\rm a}$ defined by

$$Q = {\rm Re}\{\hat{Q}\,{\rm e}^{-{\rm i}\omega t}\} = {\rm Re}\left\{ {\rm e}^{-{\rm i}\omega t} \iint_{S_{\rm C}} \left. \frac{\partial \Phi}{\partial z} \right|_{z=0} {\rm d}S \right\}, \tag{8.2}$$

and $p_{\rm a} = {\rm Re}(\hat{p}_{\rm a}\,{\rm e}^{-{\rm i}\omega t})$ with Φ being the spatial amplitude of the total velocity potential and $S_{\rm C}$ the water surface inside the column. D is the diameter of the turbine blades, N the rate of turbine rotation in r.p.m., assumed to be constant for simplicity, $\rho_{\rm a}$ the mean air density, $c_{\rm a}$ the sound speed in air, V_0 the volume of air chamber in the column and K is an empirical characterizing the turbine.[4]

Now, Φ is the sum of diffraction (φ) and radiation (ϕ) potential amplitudes to be defined later, and $\hat{Q}$ is the sum of corresponding flux rates $\hat{Q}^{\rm D}$ and $\hat{Q}^{\rm R}$, i.e.

$$\Phi = \varphi + \phi; \quad \hat{Q} = \hat{Q}^{\rm D} + \hat{Q}^{\rm R}, \tag{8.3}$$

where

$$\hat{Q}^{\rm D} = \iint_{S_{\rm C}} \left. \frac{\partial \varphi}{\partial z} \right|_{z=0} {\rm d}S \equiv \Gamma A, \tag{8.4}$$

[4]For the OWC system with one turbine on Pico Island, Portugal, $K = 3$–4.

with A being the incident wave amplitude. Thus, Γ is the diffraction flux factor Γ for unit wave amplitude. The radiation flux rates can be written as

$$\hat{Q}^{\mathrm{R}} = \iint_{S_{\mathrm{C}}} \left.\frac{\partial \phi}{\partial z}\right|_{z=0} \mathrm{d}S = -(\mathcal{B} - \mathrm{i}\mathcal{C})\hat{p}_{\mathrm{a}}, \tag{8.5}$$

where the real coefficients $\mathcal{B}$ represent the radiation damping coefficient and $\mathcal{C}$ the added compliance that plays the same role as the added mass coefficient of a rigid floating body [28]. The coefficients Γ, $\mathcal{B}$ and $\mathcal{C}$ are to be found from the solutions of the diffraction and radiation problems.

From (8.1) and (8.5), one can solve $\hat{p}_{\mathrm{a}}$ in terms of Γ,

$$\frac{\hat{p}_{\mathrm{a}}}{A_0} = \frac{\Gamma}{[(KD/N\rho_{\mathrm{a}}^0 + \mathcal{B}) - \mathrm{i}(\mathcal{C} + (\omega V_0/c_{\mathrm{a}}^2\rho_{\mathrm{a}}^0))]}. \tag{8.6}$$

The period average of power extracted is

$$P = \overline{\frac{\mathrm{d}(\rho_{\mathrm{a}} V)}{\mathrm{d}t}\frac{p_{\mathrm{a}}}{\rho_{\mathrm{a}}^0}} = \frac{KD}{2N\rho_{\mathrm{a}}}|\hat{p}_{\mathrm{a}}|^2. \tag{8.7}$$

The dimensionless capture width or efficiency is then

$$kL = \frac{P}{\rho g A_0^2 C_{\mathrm{g}}/2k} = \frac{khg}{C_{\mathrm{g}}\sqrt{g/h}}\frac{\chi|\tilde{\Gamma}|^2}{(\chi + \tilde{\mathcal{B}})^2 + (\tilde{\mathcal{C}} - \beta)^2}, \tag{8.8}$$

where the following dimensionless parameters $\tilde{\mathcal{B}}$, $\tilde{\mathcal{C}}$ and $\tilde{\Gamma}$ are used:

$$\mathcal{B} = \tilde{\mathcal{B}}\frac{h}{\rho_\omega\sqrt{g/h}}, \quad \mathcal{C} = \tilde{\mathcal{C}}\frac{h}{\rho_\omega\sqrt{g/h}}, \quad \Gamma = \tilde{\Gamma}\frac{hg}{\sqrt{g/h}}, \tag{8.9}$$

and

$$\chi = \frac{\rho_{\mathrm{w}} KD\sqrt{g/h}}{\rho_{\mathrm{a}} Nh} \quad \text{and} \quad \beta = -\left(\frac{\omega V_o \rho_{\mathrm{w}}\sqrt{g/h}}{c_{\mathrm{a}}^2\rho_{\mathrm{a}} h}\right). \tag{8.10}$$

In particular, χ characterizes the turbine (power-takeoff) system, while β is analogous to a negative spring constant, and is proportional to the chamber volume V_0.

The diffraction problem can be divided into two parts. The first is owing to diffraction by a solid column at the tip of a wedge, and can be solved explicitly. The second accounts for the oscillations inside and the continuity of normal velocity and pressure at the opening. For the radiation problem, one considers the oscillatory forcing on the free surface by a spatially uniform air pressure. For this idealized geometry, these linear problems can be solved by eigenfunction expansions and relatively straightforward computations [24–26]. For more realistic geometry involving complex bathymetry, strictly numerical methods must be employed and are available.

(*b*) *Hydrodynamic coefficients for a convex corner*

Let us examine the case of $\nu = 3/2$, so that the wedge is a convex corner of right. The column radius is allowed to be moderately large so that a few higher modes can be excited inside the chamber in addition to the Helmholtz mode.

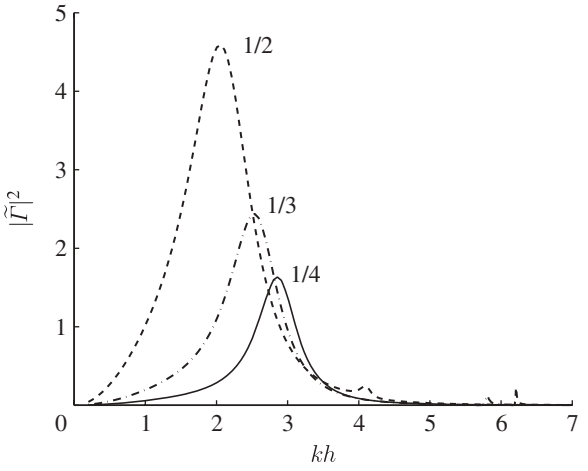

Figure 13. Diffraction flux coefficient as a function of kh. Solid line: $a/h = 1/4$; dashed and dotted line: $a/h = 1/3$; dashed line: $a/h = 1/2$. All for $d/h = 0.2$ and $\alpha = \pi/4$. Coast angle $= 3\pi/2$, i.e. $\nu = 3/2$. Adapted from Falnes & Budal [16].

Figure 13 shows the vertical flux factor $|\tilde{\Gamma}|^2$ due to diffraction for a wide range of kh for a fixed incidence angle $\alpha = \pi/4$ and three column radii: $a/h = 1/2$, 1/3,1/4.

For the smallest column, $a/h = 1/4$, there is only one resonance peak in the computed range of kh. For the larger columns, signs of more peaks at higher frequencies appear. These peaks correspond to the natural modes in a closed cylinder, $J_n(k_m r)(\cos n\theta, \sin n\theta)$, where $k_m a = j'_{nm}$ is the mth eigenvalue of $J'_n(j'_{nm}) = 0$. As a/h decreases, the highest peak shifts towards higher frequency and diminishes in intensity.

Figure 14 shows the dependence of the radiation damping $\tilde{\mathcal{B}}$ and added compliance coefficients $\tilde{\mathcal{C}}$ on kh. As a/h increases, more resonance peaks appear in the damping coefficient within the computed range of kh. These peaks occur at the same values of kh as those of Γ. It has been confirmed that the first peak at $kh = 2.18$ (i.e. $ka = 1.09$) is dominated by the Helmholtz mode modified slightly by the sloshing mode proportional to $\cos\theta$. The second peak at $kh = 4.10$ or $ka = 2.05$ is dominated by the sloshing mode, which is close to the eigenvalue $j'_{11} = 1.84118$ of the natural mode $\alpha J_1(k_{11} r)\cos(\theta) + \beta J_1(k_{11} r)\sin(\theta)$ in a closed circular cylinder. The third peak occurs at $kh = 6.34$ or $ka = 3.17$, which is close to $j'_{21} = 3.05424$, i.e. close to the natural mode $\alpha J_2(k_{21} r)\cos(2\theta) + \beta J_2(k_{21} r)\sin(2\theta)$. The free surface resembles a saddle. The existence of multi-resonant peaks is the consequence of large radius, and has been studied before for wave power absorption by an OWC in a sufficiently large harbour along a coast [29].

Note next that $\tilde{\mathcal{C}}$ is negative over certain range of frequencies; this is a distinctive feature of OWCs, similar to a moon pool. For the smallest column $a/h = 1/4$, the curve of $\tilde{\mathcal{B}}$ has only one peak of resonance in the range of kh examined. For larger $a/h = 1/3$ and 1/2, two and three peaks are evident. The peaks are higher and sharper for the larger radius. For the largest column with $a/h = 1/2$, the three peaks are at the same values of kh as $\tilde{\mathcal{B}}$.

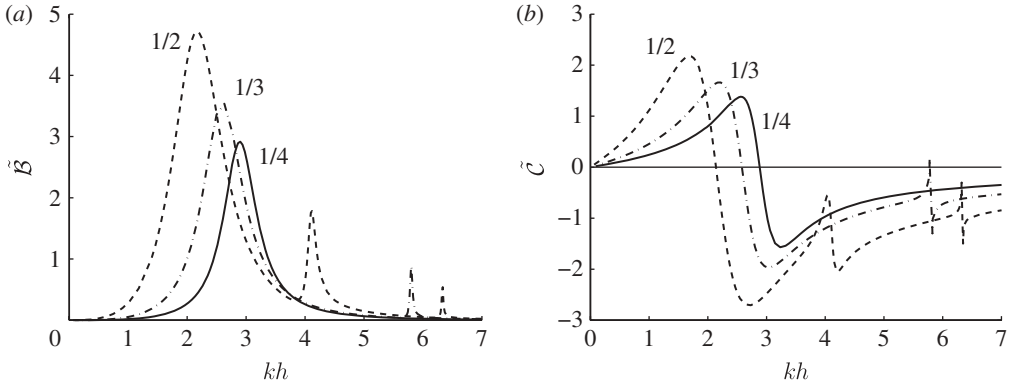

Figure 14. Effects of a/h on the (a) radiation damping and (b) added compliance coefficients. Solid line: $a/h = 1/4$; dashed-dotted line: $a/h = 1/3$; dashed line: $a/h = 1/2$. In all cases, $d/h = 0.2$. Adapted from Lovas *et al.* [26].

(*c*) *Optimization schemes*

Once the dimensions of an OWC are chosen, the factors $\Gamma, \mathcal{B}$ and $\mathcal{C}$ are fixed functions of ω of kh. Only the turbine and elasticity parameters χ and β can be controlled to maximize the efficiency. Of the two, β is the less easy to manipulate, once the volume of the air chamber V_0 is chosen. However, it may be possible to install many small turbines with adjustable blades or to use other devices to control the parameter χ over a wide range of frequencies. We now explore the theoretical potential of two strategies for maximizing the efficiency kL: (i) optimization with limitless control and (ii) optimization with limited control of the power-takeoff system.

As a preliminary, let us first choose to optimize only for one frequency. Extremizing kL with respect to β and χ separately leads to the familiar criteria

$$\beta(\omega) = \tilde{\mathcal{C}}(\omega) \quad \text{and} \quad \chi(\omega) = \tilde{\mathcal{B}}(\omega), \tag{8.11}$$

i.e. resonance and equality of radiation and extraction rates. Under these conditions, (8.8) becomes

$$kL_{\max} = \frac{gkh}{C_{\mathrm{g}}\sqrt{g/h}} \frac{|\tilde{\Gamma}(\alpha)|^2}{4\tilde{\mathcal{B}}}. \tag{8.12}$$

The following reciprocity relation can be derived for an OWC on a wedge, by a simple modification of an earlier study [28] for an open sea and the study by Evans [30] for a straight coast,

$$\tilde{\mathcal{B}} = \frac{kh^2\sqrt{g/h}}{8\pi C_{\mathrm{g}}} \int_0^{\nu\pi} |\tilde{\Gamma}(\theta)|^2 \, \mathrm{d}\theta. \tag{8.13}$$

Calculating $\hat{Q}^{\mathrm{D}}$, hence $\tilde{\Gamma}$, according to (8.4), we obtain the maximum normalized capture length

$$kL_{\max}(\alpha) = \frac{2\pi|\tilde{\Gamma}(\alpha)|^2}{\int_0^{\nu\pi} |\tilde{\Gamma}(\theta)|^2 \, \mathrm{d}\theta}. \tag{8.14}$$

These features are essentially the same as those of a simple buoy.

The averaged maximum capture length over all angles of incidence can be used as a measure of the overall efficiency for one frequency,

$$\overline{kL}_{\max} = \frac{1}{\nu\pi}\int_0^{\nu\pi} kL_{\max}(\alpha)\,\mathrm{d}\alpha = \frac{2}{\nu}. \tag{8.15}$$

In particular, it is equal to unity for a thin breakwater ($\nu = 2$) and is unaffected by the presence of the breakwater as found earlier [24], and equal to 2 for a straight coastline ($\nu = 1$, [25]). In general, $\overline{kL}_{\max}$ increases monotonically with decreasing ν. This is heuristically reasonable, since for a smaller opening angle $\nu\pi$, the incident wave energy is channelled more towards the OWC. Less energy is lost owing to radiation forced by the chamber pressure. In contrast, an OWC in the open sea scatters away most of the incident wave energy in all directions, and produces greater radiation loss. The reduction of radiation damping as ν decreases is borne out later by comparing the computed $\tilde{\mathcal{B}}$ for different ν.

It must be emphasized that for fixed chamber and column dimensions and a simple turbine system, the above maximum can only be attained for a single resonance frequency.

In the first (ideal) strategy, we assume β to be fixed and choose the best extraction coefficient χ to extremize kL for all frequencies. The condition for ideal optimum is

$$\chi_{\mathrm{opt}}(\omega) = \sqrt{\tilde{\mathcal{B}}^2 + (\tilde{\mathcal{C}} - \beta)^2}. \tag{8.16}$$

With this result and the reciprocity relation (8.13), (8.8) gives the ideal optimum capture length,

$$kL_{\mathrm{opt}} = \frac{8\pi\tilde{\mathcal{B}}\sqrt{\tilde{\mathcal{B}}^2 + (\tilde{\mathcal{C}} - \beta)^2}\,|\tilde{I}|^2}{\left[\left(\sqrt{\tilde{\mathcal{B}}^2 + (\tilde{\mathcal{C}} - \beta)^2} + \tilde{\mathcal{B}}\right)^2 + (\tilde{\mathcal{C}} - \beta)^2\right]\int_0^{\nu\pi} |\tilde{I}(\alpha')|^2\,\mathrm{d}\alpha'}. \tag{8.17}$$

Note that $kL_{\mathrm{opt}} \le kL_{\max}$ in general. Equality holds only if $\tilde{\mathcal{C}}(\omega) = \beta(\omega)$, which is realizable only for one frequency. In the following subsection, we examine the ideal efficiency for four coasts: a breakwater [24], a straight coast [25], a convex corner and a concave corner of right angle [26].

A second and likely more practical strategy is to allow χ only a few values over separate frequency ranges. Efficiencies by both *ideal* and *practical* strategies of optimization will be compared for one depth of $h = 10\,\mathrm{m}$. In subsequent examples, β is calculated for $\rho_{\mathrm{w}}/\rho_{\mathrm{a}} = 1000$, $g = 9.81\,\mathrm{m\,s^{-2}}$, $c_{\mathrm{a}} = 340\,\mathrm{m\,s^{-1}}$.

(*d*) *Ideal optimization*

Let us consider the special case of $\nu = 3/2$ so that the coastline forms a convex corner of right angle. The angle of incidence is fixed at $\alpha = \pi/2$, and the chamber volume $V_0 = \pi a^2 h$. The calculated optimum capture length $(kL)_{\mathrm{opt}}$ and the optimal turbine parameter χ_{opt} are shown for three values of a/h in figure 15. For the smallest column with $a/h = 1/4$, only the lowest modes are resonated within the computed range of kh, corresponding to the two maxima

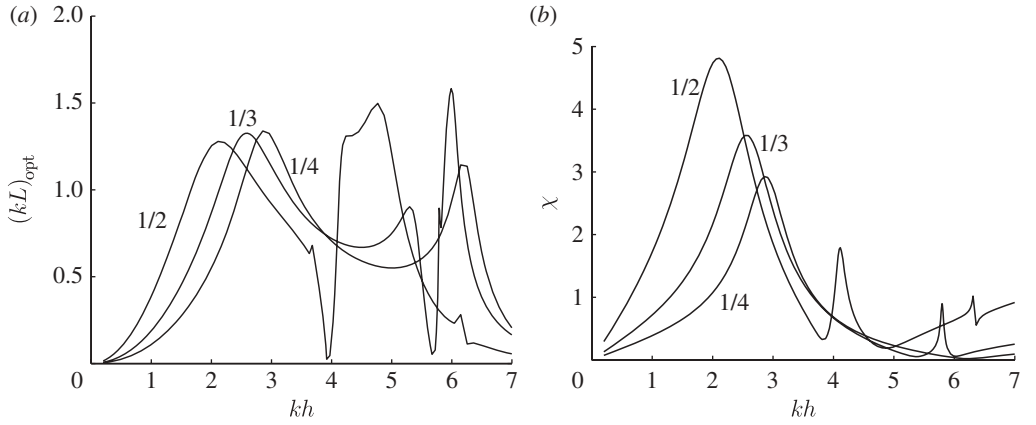

Figure 15. (*a*) Optimal capture length and (*b*) the corresponding turbine parameter as functions of kh for $a/h = 1/2$, $1/3$ and $1/4$. For all cases $\nu = 3/2$, $\alpha = \pi/2$, $d/h = 0.2$ and $V_0 = \pi a^2 h$. Adapted from Lovas *et al.* [26].

of kL. For the largest radius, four modes can be excited and hence four maxima. As a/h decreases, the efficiency curve becomes flatter and the resonance peaks are lower. The peak frequencies increase with decreasing a/h.

Note that to achieve optimum by this strategy, the turbine parameter must be varied significantly for all frequencies. This may be very difficult to realize in practice.

As seen in (8.10), the effective spring constant β is proportional to the chamber height or volume V_0. Can a fixed value of V_0 be suitably chosen for good performance? Consider the smallest column radius with $a/h = 1/4$. Figure 16 displays the results for $\alpha = \pi/2$ only, as results for other incidence angles are quite similar. The added mass curve of $\tilde{\mathcal{C}}(\omega)$ versus kh is in general shaped like the letter N, which crosses the zero line. If $V_0 = 0$, as in figure 16*a*, the β curve is horizontal and intersects with the $\tilde{\mathcal{C}}$ curve only once near $kh \approx 3$. Correspondingly, $(kL)_{\rm opt}$ reaches a single maximum. As V_0 increases, the β curve is slanted downwards. The negative branch of $\tilde{\mathcal{C}}$ now intersects with β twice, as seen in figure 16*b*, giving rise to two well-separated peaks of $(kL)_{\rm opt}$, hence broadening the bandwidth of large capture width and high efficiency. As V_0 increases further, the two intersections eventually merge and the bandwidth shrinks. Beyond $V_0 = 5\pi a^2 h$, intersection no longer occurs and the capture width drops to a small local maxima, as seen in figure 16*d*. Similar features are found for the larger columns with $a/h = 1/3$ and $1/2$. This shows that the bandwidth of high extraction efficiency can be widened by proper choice of the column height. In subsequent computations, we set $V_0 = \pi a^2 h$.

By the same scheme of optimization, the effects of coastal geometries on the performance of an OWC with the same column dimensions ($a/h = 1/4$, $d/h = 0.2$ and $V_0 = \pi a^2 h$) are compared in figure 17 for the four coastlines. The optimal capture length is seen to be smaller for larger opening angles (larger ν), consistent with (8.15). The variation of χ with respect to kh is smaller and smoother, implying less difficulty in the design of the control system.

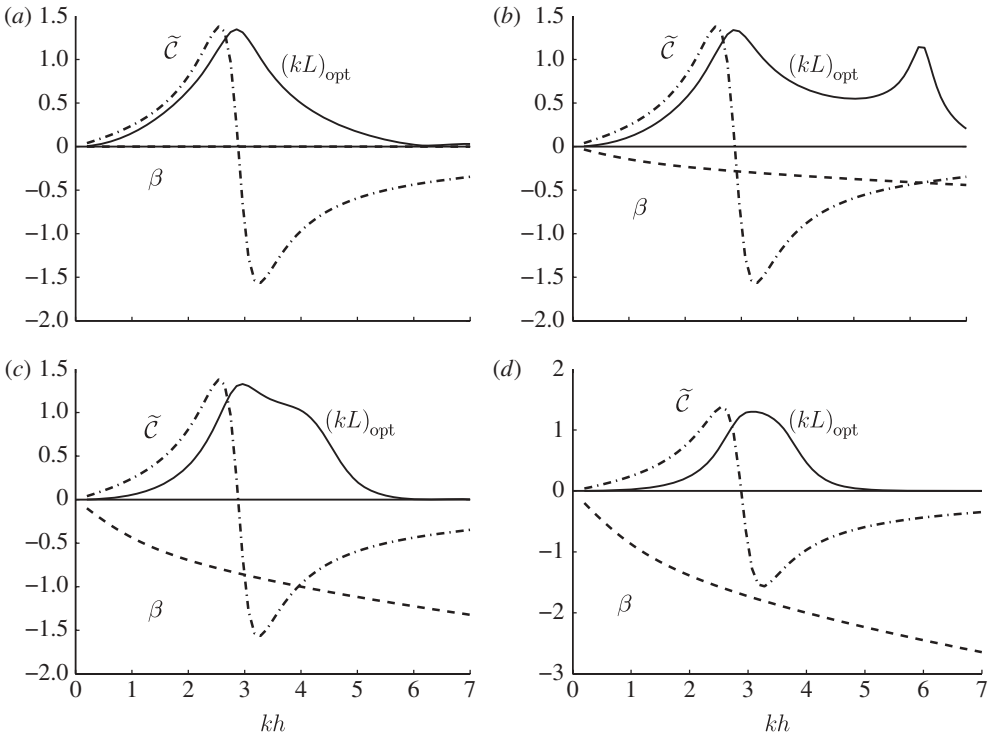

Figure 16. Optimal capture length (solid line), added mass coefficient (dashed line) and β (dashed-dotted line) versus kh for different pneumatic chamber volume V_0. (*a*) $V_0 = 0$, (*b*) $V_0 = \pi a^2 h$, (*c*) $V_0 = 3\pi a^2 h$, (*d*) $V_0 = 6\pi a^2 h$. For all cases, $\nu = 3/2$, $\alpha = \pi/2$, $a/h = 1/4$, $d/h = 0.2$, $h = 10\,\mathrm{m}$. Adapted from Lovas *et al.* [26].

(*e*) *Practical optimization*

As seen in figure 15, the ideal optimization scheme requires the turbine parameter χ to vary drastically over the frequency range. Let us examine the second strategy, which is less ambitious and likely more feasible.

Consider first an OWC at the convex corner of right angle. First, we compute $(kL)_{\mathrm{opt}}$ according to the ideal strategy, and identify $(kh)_1$ and $(kh)_2$ at two resonant peaks where $\beta = \tilde{\mathcal{C}}$. The corresponding turbine parameters χ_1, χ_2 are found from $\chi(\omega) = \tilde{\mathcal{B}}$. We now choose χ to be piece-wise constant, i.e. $\chi = \chi_1$ for $0 < kh < (kh)_*$ and $\chi = \chi_2$ for $kh > (kh)_*$, where $(kh)_*$ can be decided by trial and error. With this strategy, the new curves of the capture width, $(kL)_{\mathrm{prac}}$, are recomputed. In the numerical example, we choose a column with $a/h = 1/2$, $d/h = 0.2$ and the angle of incidence at $\pi/2$. For this configuration, $\chi_1 = 4.812$ and $\chi_2 = 0.202$ from two resonance peaks at $(kh)_1 = 2.11$ and $(kh)_2 = 4.77$. Choosing $(kh)^* = 3.97$, the predicted $(kL)_{\mathrm{prac}}$ and the corresponding χ are shown in figure 18 by solid lines. For comparison, the corresponding curves by ideal optimization are shown by dashed lines. Clearly, the capture width by the practical strategy is not far from that by the ideal one.

Next, consider a concave corner with the same column parameters and a different angle of incidence $\alpha = \pi/4$. Figure 19 shows the comparison of two

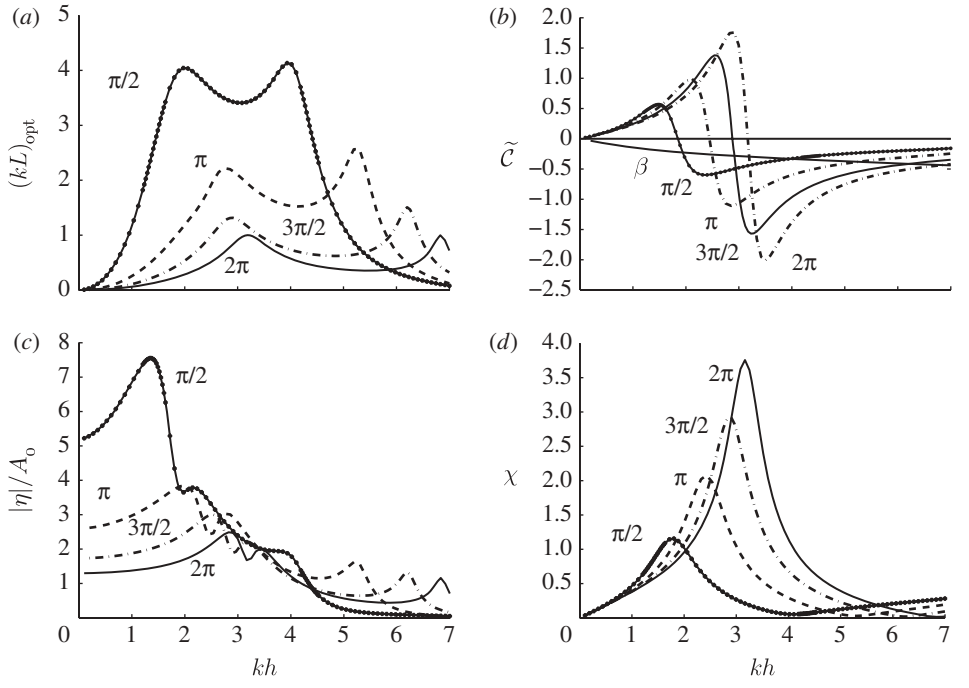

Figure 17. Comparison for different coastline angles $\nu\pi$. Solid line with point markers: $\pi/2$ (concave corner); dashed line: π (straight coast); dashed-dotted line: $3\pi/2$ (convex corner); solid line: 2π (breakwater). (*a*) Capture length, (*b*) added compliance coefficient, (*c*) free-surface elevation, (*d*) turbine parameter. In all cases, $\nu = 3/2$, $\alpha = \pi/4$, $d/h = 0.2, a/h = 1/4$ and $V_0 = \pi a^2 h$. Adapted from Lovas *et al.* [26].

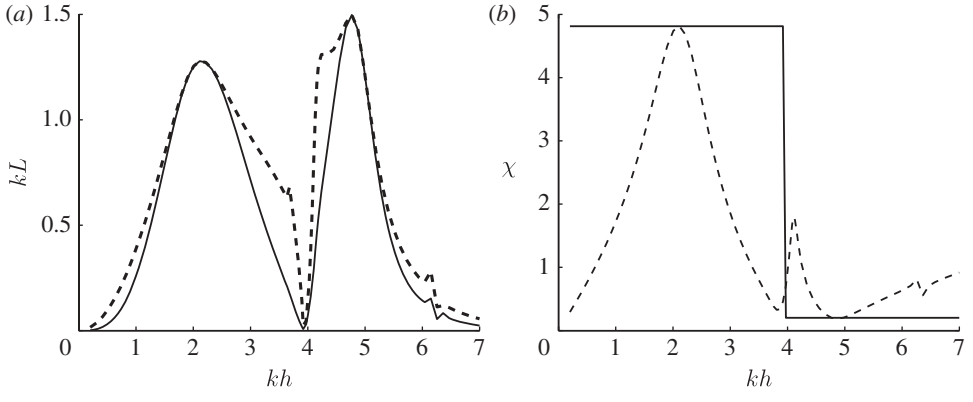

Figure 18. Comparison of practical versus ideal optimizations for an OWC at a convex corner ($\nu = 3/2$) with $a/h = 1/2, d/h = 0.2$ and $\alpha = \pi/2$. (*a*) Capture length kL. (*b*) Turbine parameter χ. Practical optimization (solid line) and ideal optimization (dashed line). Adapted from Lovas *et al.* [26].

strategies. Here, $\chi_1 = 0.604$, $\chi_2 = 1.181$ and $(kh)^* = 3.68$. Again, the two strategies give roughly the same capture length for almost all frequencies. This encouraging result can be understood from figure 19*b*, where χ_{opt} and χ_{prac} coincide at eight values of kh.

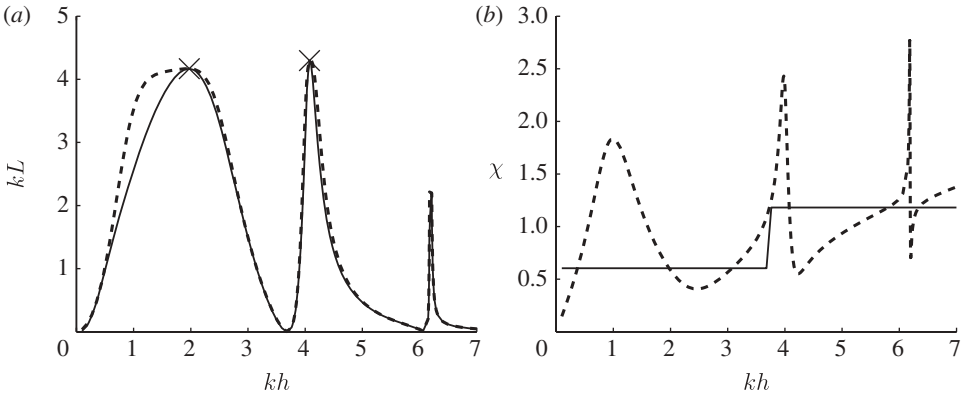

Figure 19. Comparison of practical versus ideal optimizations for an OWC at a concave corner ($\nu = 3/2$) with $a/h = 1/2, d/h = 0.2, \alpha = \pi/4$ and $V_0 = \pi a^2 h$. (*a*) Optimal capture length kL. (*b*) Turbine parameter χ. Practical optimization (solid line) and ideal optimization (dashed line). Adapted from Lovas *et al.* [26].

9. Concluding remarks

We have reviewed the hydrodynamics of two representative WECs that transfer sea wave energy to the power-takeoff via the oscillatory motion of the system. The common principle for optimum design is shown to be impedance matching, whereby the system geometry produces resonance at the design frequency and the extraction rate equal to the rate of radiation damping. We have also discussed a compact array of small buoys that are not resonated, hence do not suffer the inherent bandwidth limit of a large buoy. For an OWC, it is suggested that a proper choice of the air chamber height and a modest control of the power-take off system may broaden the bandwidth of high efficiency, Finally, a concave coastline can help channel the incident wave towards the converter and increase the capture width.

Many important topics such as the randomness of incident waves, dynamic coupling with the mooring system and the effects of local bathymetry are not covered here, but they can, within the framework of the linear potential theory, be dealt with by existing computational means. A challenge of the utmost urgency is to model the nonlinear dynamics of the violent sea. Greater efforts by hydrodynamicists and closer collaborations with designers and planners are needed to expedite the full utilization of wave power.

Liberal use has been made of the results in recent publications with my collaborators. Herve Martin-Rivas, Xavier Garnaud and Stéphanie Lovas. The authors thank the Earth Systems Initiative of the Massachusetts Institute of Technology for a grant supporting parts of the research reported here.

References

1 Salter, S. 1974 Wave power. *Nature* **249**, 720–724. (doi:10.1038/249720a0)
2 Budal, K. & Falnes, J. 1975 A resonant point absorber of ocean-wave power. *Nature* **256**, 478–479. (doi:10.1038/256478a0)
3 French, M. J. 1979 The search for low cost energy and the flexible bag device. In *Proc. 1st. Symp. Wave Energy Utilization, Gothenburg, Sweden*, pp. 364–377.

4 Farley, F. & Rainey, R. C. T. Anaconda. 2006 See http://www.bulgewave.com.
5 McCormick, M. E. 1981 *Ocean wave energy conversion*. New York, NY: Wiley Interscience.
6 Mei, C. C. 1983 *Applied dynamics of ocean surface waves*. New York, NY: Wiley Interscience.
7 Mei, C. C., Stiassnie, M. & Yue, D. K.-P. 2005 *Theory and application of ocean surface waves*. Singapore: World Scientific.
8 Falnes, J. 2002 *Ocean waves and oscillating systems*. Cambridge, UK: Cambridge University Press.
9 Cruz, J. 2008 *Ocean wave energy*. Berlin, Germany: Springer.
10 Evans, D. V. 1981 Power from water waves. *Ann. Rev. Fluid Mech.* **13**, 157–187. (doi:10.1146/annurev.fl.13.010181.001105)
11 Falcão, A. F. de O. 2010 Wave energy utilisation: a review of the technologies. *Renew. Sustain. Energy Rev.* **14**, 899–918. (doi:10.1016/j.rser.2009.11.003)
12 Thorpe, T. W. 1999 A brief review of wave energy. ETSU-R120. Report to UK Department of Trade and Industry.
13 Newman, J. N. 1976 The interaction of stationary vessels with regular waves. In *Proc. 11th Symposium on Naval Hydrodynamics, London, UK*, pp. 491–501.
14 Newman, J. N. 1962 The exciting forces on fixed bodies in waves. *J. Ship Res.* **6**, 10–17.
15 Budal, K. 1977 Theory for absorption of wave power by a system of interacting bodies. *J. Ship Res.* **21**, 248–253. (doi:10.1016/S0141-1187(82)80026-6)
16 Falnes, J. & Budal. K. 1982 Wave-power absorption by parallel rows of interacting oscillating bodies. *Appl. Ocean Res.* **4**, 194–207. (doi:10.1016/S0141-1187(82)80026-6)
17 Falnes, J. 2002 Optimum control of oscillation of wave-energy converters. *J. Offshore Polar Eng.* **12**, 147–155.
18 Falcão, A. F. de O. 2008 Phase control through load control of oscillating-body wave energy converters with hydraulic PTO system. *Ocean Eng.* **35**, 358–366. (doi:10.1016/j.oceaneng.2007.10.005)
19 Garnaud, X. & Mei, C. C. 2009 Wave power extraction by a compact array of buoys. *J. Fluid Mech.* **635**, 389–413. (doi:10.1017/S0022112009007411)
20 Garnaud, X. & Mei, C. C. 2010 Comparison of a large buoy with a compact array of small buoys for wave energy extraction. *J. Inst. Eng. Technol.* **32**, 267–283.
21 Falcão, A. F. de O. 2002 Wave-power absorption by a periodic linear array of oscillating water columns. *Ocean Eng.* **29**, 1163–1186. (doi:10.1016/S0029-8018(01)00076-2)
22 Falnes, J. 1984 Wave-power absorption by an array of attenuators oscillating with unconstrained amplitudes. *Appl. Ocean Res.* **6**, 16–22. (doi:10.1016/0141-1187(84)90024-5)
23 Garnaud, X. & Mei, C. C. 2010 Bragg scattering and wave-power extraction by an array of small buoys. *Proc. R. Soc. A* **466**, 79–106. (doi:10.1098/rspa.2009.0458)
24 Martin-Rivas, H. & Mei, C. C. 2008 Wave power extraction from an oscillating water column at the tip of a breakwater. *J. Fluid Mech.* **626**, 395–414. (doi:10.1017/S0022112009005990)
25 Martin-Rivas, H. & Mei, C. C. 2009 Wave power extraction from an oscillating water column along a straight coast. *Ocean Eng.* **36**, 426–433. (doi:10.1016/j.oceaneng.2009.01.009)
26 Lovas, S., Mei, C. C. & Liu, Y. M. 2010 Oscillating water column at a coastal corner for wave power extraction. *Appl. Ocean Res.* **32**, 267–283. (doi:10.1016/j.apor.2010.06.004)
27 Sarmento, A. J. N. A. & Falcão, A. F. de O. 1985 Wave generation by an oscillating surface-pressure and its application in wave-energy extraction. *J. Fluid Mech.* **150**, 467–485. (doi:10.1017/S0022112085000234)
28 Evans, D. V. 1982 Wave-power absorption by systems of oscillating surface pressure distributions. *J. Fluid Mech.* **114**, 481–499. (doi:10.1017/S0022112082000263)
29 Malmo, O. & Reitan, A. 1986 Development of the Kvaerner multi-resonant OWC. In *Proc. IUTAM Symp. Hydrodynamics of Ocean Wave-Energy Utilization, Lisbon, Portugal, 8–11 July 1985* (eds. D. V. Evans & A. F. de Falcao), pp. 57–67. Berlin, Germany: Springer.
30 Evans, D. V. 1988 Maximum efficiency of wave-energy devices near coast lines. *Appl. Ocean Res.* **10**, 162–164. (doi:10.1016/S0141-1187(88)80016-6)